

1 **A genetic particle filter scheme for univariate snow cover**  
2 **assimilation into Noah-MP model across snow climates**

3 Yuanhong You<sup>1,3</sup>, Chunlin Huang<sup>2</sup>, Zuo Wang<sup>1</sup>, Jinliang Hou<sup>2</sup>, Ying Zhang<sup>2</sup>, Peipei Xu<sup>1</sup>  
4

5 <sup>1</sup>Anhui Normal University, School of Geography and Tourism, Key Laboratory of Earth Surface  
6 Processes and Regional Response in the Yangtze-Huaihe River Basin of Anhui Province, Wuhu,  
7 241002, China  
8

9 <sup>2</sup>Northwest Institute of Eco-Environment and Resources, Chinese Academy of Sciences, Lanzhou,  
10 730000, China  
11

12 <sup>3</sup>Engineering Technology Research Center of Resource Environment and GIS, Wuhu, 241002,China  
13  
14  
15  
16

17 Corresponding author: Chunlin Huang, Key Laboratory of Remote Sensing of Gansu Province,  
18 Northwest Institute of Eco-Environment and Resources, Chinese Academy of Sciences, Lanzhou,  
19 Gansu, 730000, China. (huangcl@lzb.ac.cn)  
20  
21  
22

## 23 **Abstract**

24 Accurate snowpack simulations are critical for regional hydrological predictions, snow  
25 avalanche prevention, water resource management, and agricultural production, particularly during  
26 the snow ablation period. Data assimilation methodologies are increasingly being applied for  
27 operational purposes to reduce the uncertainty in snowpack simulations and enhance their predictive  
28 capabilities. This study aims to investigate the feasibility of using Genetic Particle Filter (GPF) as a  
29 snow data assimilation scheme designed to assimilate ground-based snow depth (SD) measurements  
30 across different snow climates. We employed the default parameterization scheme combination  
31 within the Noah-MP model as the model operator in the snow data assimilation system to evolve  
32 snow variables and evaluated the assimilation performance of GPF using observational data from  
33 sites with different snow climates. We also explored the impact of measurement frequency and  
34 particle number on the filter updating of the snowpack state at different sites and the results of generic  
35 resampling methods compared to the genetic algorithm used in the resampling process. Our results  
36 demonstrate that GPF can be used as a snow data assimilation scheme to assimilate ground-based  
37 measurements and obtain satisfactory assimilation performance across different snow climates. We  
38 found that particle number is not crucial for the filter's performance, and 100 particles are sufficient  
39 to represent the high dimensionality of the point-scale system. The frequency of measurements can  
40 significantly affect the filter updating performance, and dense ground-based snow observational data  
41 always dominate the accuracy of assimilation results. Compared to generic resampling methods, the  
42 genetic algorithm used to resample particles can significantly enhance the diversity of particles and  
43 prevent particle degeneration and impoverishment. Finally, we concluded that the GPF is a suitable  
44 candidate approach for snow data assimilation and is appropriate for different snow climates.

## 45 **1. Introduction**

46 Understanding snowpack dynamics is crucial for water resource management, agricultural  
47 production, avalanche prevention and flood preparedness in snow dominated regions (Piazzini et al.,  
48 2019; Pulliainen et al., 2020). As a special land surface type, seasonal snow cover is highly sensitive  
49 to climate change and has a significant impact on energy and hydrological processes (Barnett et al.,  
50 2005; Takala et al., 2011; Kwon et al., 2017; Che et al., 2014). On one hand, the high albedo of snow-  
51 covered surfaces can significantly reduce shortwave radiation absorption, leading to adjustments in  
52 the energy exchange between the land surface and atmosphere (You et al., 2020a; You et al., 2020b).  
53 On the other hand, the low thermal conductivity of snow cover can insulate the underlying soil, which  
54 results in reduced temperature variability and a more stable environment (Zhang et al., 2005; Piazzini  
55 et al., 2019). In addition, snowmelt is a vital source of water that plays a critical role in soil moisture,

56 runoff, and groundwater recharge (Dettinger, 2014; Griessinger et al., 2016; Oaida et al., 2019).  
57 Therefore, comprehending snow dynamics is essential for predicting snowmelt runoff, atmospheric  
58 circulation, hydrological predictions, and climate change.

59 Currently, there is a growing effort to investigate the potential of data assimilation (DA) schemes  
60 to improve snow simulations and obtain the optimal posterior estimate of the snowpack state  
61 (Bergeron et al., 2016; Piazzi et al., 2018; Smyth et al., 2020; Abbasnezhadi et al., 2021). Various DA  
62 methodologies with different degrees of complexity have been developed, resulting in diverse  
63 performance levels. Sequential DA techniques, including basic direct insertion, optimal interpolation  
64 schemes, ensemble-based Kalman filter, and particle filter, have been widely employed in real-time  
65 applications. The greatest strength of sequential DA techniques is that the model state can be  
66 sequentially updated when observational data become available (Piazzi et al., 2018). However, the  
67 direct insertion method, which replaces model predictions with observations when available, is based  
68 on the assumption that the observation is perfect and the model prior is wrong (Malik et al., 2012).  
69 This method can potentially result in model shocks due to physical inconsistencies among state  
70 variables (Magnusson et al., 2017). Although the optimal interpolation method is more advanced and  
71 takes into account observational uncertainty, it still has great limitations and is rarely used in real-  
72 time operational systems (Dee et al., 2011; Balsamo et al., 2015).

73 At a higher level are the Kalman filter and ensemble-based Kalman filter, which are most  
74 commonly used in various real-time applications. The Ensemble Kalman Filter (EnKF), which was  
75 first introduced by Evensen in 2003, uses a Monte Carlo approach to approximate error estimates  
76 based on an ensemble of model predictions. This approach does not require model linearization,  
77 making it particularly advantageous. Precisely due to this advantage, the EnKF has been widely used  
78 in snowpack prediction. For example, EnKF has been used to assimilate MODIS snow cover extent  
79 and AMSR-E SWE into a hydrological model to improve modeled SWE (Andreadis et al., 2006), as  
80 well as to assimilate MODIS fractional snow cover into a land surface model (Su et al., 2008).  
81 Moreover, the EnKF method has been used to enhance snow water equivalent estimation by  
82 assimilating ground-based snowfall and snowmelt rates, assimilation of both D-InSAR (Differential  
83 Interferometric Synthetic Aperture Radar) and manually measured snow depth data simultaneously  
84 (Yang and Li, 2021). Even though there are numerous studies have generally stated that the EnKF  
85 has an excellent assimilation performance enabling it to consistently improve snow simulations, some  
86 constraining limitations hinder the filter performance (Chen, 2003). One of the main limitations is  
87 that the EnKF assumes that the model states follow a Gaussian distribution and only considers the  
88 first and second order moments, thereby losing relevant information contained in higher-order  
89 moments (Moradkhani et al., 2005). Unfortunately, the dynamical system usually has strong  
90 nonlinearity and the involved probability distribution of system state variables is not supposed to  
91 follow a Gaussian distribution (Weerts and El Serafy, 2006). Additionally, the filter performance of

92 the EnKF is significantly influenced by the linear updating procedure, and the state-averaging  
93 operations can be particularly challenging for highly detailed complex snowpack models.

94 In order to overcome these limitations, the particle filter (PF) which also based on Monte Carlo  
95 method has been developed for non-Gaussian, nonlinear dynamic models (Gordon et al., 1993). The  
96 greatest strength of PF technique is to be free from the constraints of model linearity and error  
97 following a Gaussian distribution. This enables the successful application of the PF technique to  
98 nonlinear dynamical systems with non-Gaussian errors. Additionally, the PF technique gives weights  
99 to individual particles but leave model states untouched, which makes PF more computationally  
100 efficient than the ensemble Kalman filter and smoother techniques (Margulis et al., 2015). Thanks to  
101 these advantages, an increasing interest focuses on applying PF technique in snow data assimilation.  
102 For example, remotely sensed microwave radiance data were assimilated into a snow model to update  
103 model states using the PF technique, and the results demonstrated that the SWE simulations have  
104 great improvement (Dechant and Moradkhani, 2011; Deschamps-Berger et al., 2022). A newly PF  
105 approach proposed by Margulis et al. (2015) was used to improve SWE estimation through  
106 assimilating remotely sensed fractional snow-covered area. At basin scale, PF technique was  
107 implemented with the objective of obtaining high resolution retrospective SWE estimates (Cortes et  
108 al., 2016). The PF technique was also used to assimilate daily snow depth observations within a multi-  
109 layer energy-balance snow model to improve SWE and snowpack runoff simulations (Magnusson et  
110 al., 2017). The studies indicated above demonstrated that the assimilated snow-related in-situ  
111 measurements or the remotely sensed observation data through the PF technique can successfully  
112 update predicted snowpack dynamics, and the PF scheme is a well-performing data assimilation  
113 technique enabling to consistently improve model simulations. Nevertheless, particle degeneracy is  
114 still a potential limitation of the PF technique. It occurs when most particles have negligible weight,  
115 and only a few particles carry significant weights, which hinders a realistic sampling of the underlying  
116 probability distribution of the state (Parrish et al., 2012; Abbaszadeh et al., 2017; Abbaszadeh et al.,  
117 2018). The particle resampling has been considered to be an efficient approach that can effectively  
118 mitigate the problem of particle degeneracy. However, it may result in a sample containing many  
119 repeated points and a lack of diversity among the particles, which is referred to as sample  
120 impoverishment (Rings et al., 2012; Zhu et al., 2018). And the sample impoverishment was a tricky  
121 problem for generic resampling methods. Using intelligent search and optimization methods to  
122 mitigate the degeneracy problem may be a good choice because it can effectively avoid sample  
123 impoverishment (Park et al., 2009; Ahmadi et al., 2012; Abbaszadeh et al., 2018). The Genetic  
124 Algorithm (GA) as an intelligent search and optimization method has been known as an effective  
125 approach to mitigate the degeneracy problem and received more attention (Kwok et al., 2005; Park  
126 et al., 2009; Mechri et al., 2014). The GA applied in the particle filter, which is referred to as the  
127 genetic particle filter (GPF), has been successfully implemented to estimate parameters or states in

128 nonlinear models (Van Leeuwen, 2010; Snyder, 2011). The GPF was also used as data assimilation  
129 scheme applied to land surface model which simulates prior subpixel temperature and the results  
130 showed the GPF outperformed prior model estimations (Mechri et al., 2014). Despite a series of  
131 studies having proven that the GPF is an effective data assimilation approach, however, few studies  
132 have investigated the performance of GPF as a snow data assimilation scheme, especially in different  
133 snow climates. In view of the promising performances of GPF as a snow data assimilation scheme,  
134 this paper aims to investigate the potential of GPF in performing snow data assimilation, and the main  
135 goal of this research is to address the following issues: (1) Can the GPF be employed as a snow data  
136 assimilation scheme? (2) How is the assimilation performance of GPF in snow data assimilation  
137 across different snow climates? (3) The sensitivity of DA simulations to the frequency of the  
138 assimilated measurements and the particle number.

139 This paper is organized as follows. Section 2 introduces the study sites, the meteorological  
140 dataset, the snow module within the Noah-MP model, the calculation flow of the GPF scheme, and  
141 design of the numerical experimental. Section 3 explains the simulation results of SD using the open-  
142 loop ensemble, explores the sensitivity of the measurement frequency and ensemble size. Finally,  
143 section 4 summarizes the findings of this study.

## 144 **2. Materials and methods**

### 145 *2.1 Study sites and data*

146 With consideration of the filtering performance, which may vary in snow climates, eight  
147 seasonally snow-covered study sites with different snow climates were selected to implement  
148 numerical experimental in this study (Sturm et al., 1995; Trujillo and Molotch, 2014). These sites are  
149 distributed at different latitudes in the Northern Hemisphere, and the sites included the Arctic  
150 Sodankylä site (SDA, 179 m), located beside the Kitinen River in Finland and the upper 2 meters are  
151 frozen (Rautiainen et al., 2014); the Snoqualmie site (SNQ, 921 m) with a rain-snow transitional  
152 climate in the Washington Cascades of the USA, the SD measured by snow stakes was employed  
153 (Wayand et al., 2015); the maritime Col de Porte (CDP, 1330 m) site in the Chartreuse Range in the  
154 Rhone-Alpes region of France; the Mediterranean climate Refugio Poqueira site (ROPA, 2510 m) in  
155 Sierra Nevada Mountains of Spain and has a high evaporation rate (Herrero et al., 2009); the  
156 Weissfluhjoch site (WFJ, 2540 m) in Davos of Switzerland, and automatic SD observations used in  
157 this study (Wever et al., 2015); the continental Swamp Angel Study Plot (SASP, 3370 m) site in the  
158 San Juan Mountains of Colorado, USA; and two sites from typical snow-covered regions in China,  
159 the Altay meteorological observation site (ATY, 735.3 m) in Northern Xinjiang, China, where there  
160 is less wind in the winter season; the other one is the Mohe meteorological observation site (MOHE,  
161 438.5 m) in a county of Northeast China, which has a cold temperate continental climate and is the

162 northernmost part of China. Serially complete meteorological measurements are available and can be  
 163 used as forcing data in these sites, certainly, the downward longwave and shortwave radiation values  
 164 of MOHE were extracted from the China Meteorological Forcing Dataset (CMFD) (Chen et al, 2011),  
 165 since there are no radiation measurements in this site.

166 It is noteworthy that the spatial variance of the performance of the model is negligible since  
 167 these sites themselves are flat and the surrounding vegetation types are uniform. We have used this  
 168 data set to examine the sensitivity of simulated SD to physics options, and the results shown that the  
 169 dataset has a reliable quality. In addition, the location, the detailed information of snow climates, and  
 170 details about the dataset processing for the eight sites can be also referenced in You et al. (2020a).

## 171 *2.2 Snow module within Noah-MP model*

172 The snow partial module within Noah-MP model can be divided into up to three layers,  
 173 depending on the depth of the snow (Yang et al., 2011). The SD  $h_{snow}$  is calculated by

$$174 \quad h_{snow}^t = h_{snow}^{t-1} + \frac{P_{s,g}}{\rho_{sf}} dt . \quad (1)$$

175 where  $P_{s,g}$  is the snowfall rate at the ground surface,  $dt$  is the timestep, and  $\rho_{sf}$  is the bulk  
 176 density of the snowfall. When  $h_{snow} < 0.025$  m, the snowpack is combined with the top soil layer, and  
 177 no dependent snow layer exists. When  $0.025 \leq h_{snow} \leq 0.05$  m, a snow layer is created with a thickness  
 178 equal to SD. When  $0.05 < h_{snow} \leq 0.1$  m, the snowpack will be divided into two layers, each with a  
 179 thickness of  $\Delta z_{-1} = \Delta z_0 = h_{snow} / 2$ . When  $0.1 < h_{snow} \leq 0.25$  m, the thickness of the first layer is  
 180  $\Delta z_{-1} = 0.05$  m, and the thickness of the second layer is  $\Delta z_0 = (h_{snow} - \Delta z_{-1})$  m. When  $0.25 < h_{snow} \leq 0.45$  m,  
 181 a third layer is created, and the three thickness are:  $\Delta z_{-2} = 0.05$  m and  $\Delta z_{-1} = \Delta z_0 = (h_{snow} - \Delta z_{-2}) / 2$  m.  
 182 When  $h_{snow} > 0.45$  m, the layer thickness of the three snow layers are  $\Delta z_{-2} = 0.05$  m,  $\Delta z_{-1} = 0.2$  m,  
 183  $\Delta z_0 = (h_{snow} - \Delta z_{-2} - \Delta z_{-1})$  m. Certainly, the snow cover is highly influenced by air and ground  
 184 temperature, and the snow layer combines with the neighboring layer due to sublimation or melting  
 185 and is redivided depending on the total SD. The snow module of the Noah-MP model provides an  
 186 estimate of snow-related variables using energy and mass balance. This computing process requires  
 187 a series of meteorological forcing data, such as near-surface air temperature, precipitation, and  
 188 downward solar radiation. The snow accumulation or ablation parameterization of the Noah-MP  
 189 model is based on the mass and energy balance of the snowpack, and the snow water equivalent can

190 be calculated using the following equation:

$$191 \quad \frac{dW_s}{dt} = P_{s,g} - M_s - E. \quad (2)$$

192 where  $W_s$  is the snow water equivalent (mm),  $P_{s,g}$  is the solid precipitation ( $\text{mm s}^{-1}$ ),  $M_s$  is the  
193 snowmelt rate ( $\text{mm s}^{-1}$ ),  $E$  is the snow sublimation rate ( $\text{mm s}^{-1}$ ).

194 A snow interception model was implemented into the Noah-MP model to describe the process  
195 of snowfall intercepted by the vegetation canopy (Niu and Yang, 2004). Within this model, the  
196 snowfall rate at the ground surface  $P_{s,g}$  is then calculated by

$$197 \quad P_{s,g} = P_{s,drip} + P_{s,throu}. \quad (3)$$

198 where  $P_{s,drip}$  ( $\text{mm s}^{-1}$ ) is the drip rate of snow and  $P_{s,throu}$  ( $\text{mm s}^{-1}$ ) is the through-fall rate of snow. In  
199 the Noah-MP model, the ground surface albedo is parameterized as an area-weighted average of the  
200 albedos of snow and bare soil, and the snow cover fraction of the canopy is used to calculate the  
201 ground surface albedo, as shown in Equation (4),

$$202 \quad \alpha_g = (1 - f_{snow,g}) \alpha_{soil} + f_{snow,g} \alpha_{snow}. \quad (4)$$

203 where  $\alpha_{soil}$  and  $\alpha_{snow}$  are the albedo of bare soil and snow, respectively.  $f_{snow,g}$  is the snow cover  
204 fraction on the ground and is parameterized as a function of snow depth, ground roughness length,  
205 and snow density (Niu and Yang, 2006).

### 206 **2.3 Genetic particle filter data assimilation scheme**

207 The Bayesian recursive estimation problem is solved by the Monte Carlo approach within PF  
208 technique, making this scheme appropriate for nonlinear system with a non-Gaussian probability  
209 distribution (Magnusson et al., 2017). The basic concept of PF technique is to use a large number of  
210 randomly generated realizations (i.e., particles) of the system state to represent the posterior  
211 distribution. Meanwhile, the particles are propagated forward in time as the model evolves. The  
212 weights associated with the particles are updated based on the likelihood of each particle's simulated  
213 proximity to the real observation. The weight of the particles can be updated as follows:

$$214 \quad w_t^i = w_{t-1}^i p(z_t | x_t^i). \quad (5)$$

215 where  $w_{t-1}^i$  is the weight of  $i$  th particle at time  $t-1$  and the weight is updated by the likelihood  
216 function  $p(z_t | x_t^i)$ , which measures the likelihood of a given model state with respect to the  
217 observation  $z_t$ . The observation errors are generally assumed to follow a Gaussian distribution, and

218 the chosen likelihood function represents this assumption. In this study, we employed a normal  
219 probability distribution to serve as likelihood function:

$$220 \quad p(z_t | x_t^i) = N(z_t - x_t^i, \sigma). \quad (6)$$

221 where  $N$  represents the normal probability distribution of the residuals between observed,  $z_t$ , and  
222 simulated,  $x_t$ . Finally, the weights of the updated model state would be normalized, and the  
223 assimilated value of model state is the weighted average of all particles at time  $t$ . Although the  
224 particle filter has been widely applied in various nonlinear systems, the particle degeneracy and  
225 impoverishment in particle filter are still the fatal limitations need to be urgently addressed. To  
226 address the degeneration problem in PF technique, traditional resampling methods like multinomial  
227 resampling, systematic resampling were employed to resample the particles if the effective sample  
228 size,

$$229 \quad N_{eff} = 1 / \sum_{i=1}^N (w_t^i)^2. \quad (7)$$

230 fell below a specified number. Where  $N$  is the ensemble size and  $w_t^i$  is the normalized weights  
231 defined in Equation (5). To be honest, traditional resampling methods can effectively mitigate the  
232 problem of particle degeneracy by resampling high-quality particles. However, after multiple  
233 iterations, these methods often lead to a serious lack of diversity among particles, which is known as  
234 the particle impoverishment problem. To mitigate both of these issues simultaneously, we employed  
235 the genetic algorithm (GA) to resample the particles, resulting in the genetic particle filter algorithm  
236 (GPF). The GA is inspired by Darwin's theory of evolution and emphasizes the principle of survival  
237 of the fittest. In fact, in the resampling phase, the fitness of particles should be reselected according  
238 to the theory of particle filtering. Selection, crossover, and mutation are major steps used to simulate  
239 population evolution. As shown in Figure 1, these three operators are utilized to produce better  
240 offspring and improve the overall population fitness, with the aim of preventing particle degeneracy  
241 and impoverishment. These operators will be used to improve particle fitness when it falls below a  
242 threshold value. The three operators are described below.

243 **Selection mechanism:** At the time of assimilation, the selection operator will preferentially select the  
244 particles that are close to the observed SD. This process is usually achieved by sorting the fitness  
245 value of all particles and selecting a certain proportion of particles. Here, we calculated the survival  
246 rate of all individuals and sorted them in ascending order. The top fifth percentile of particles were  
247 considered high-quality particles and were selected as parents in genetic algorithm. This ensures that  
248 fit individuals can be delivered to the next generation group. The survival rate of particles can be  
249 calculated using the following equation:



250

$$P(x_{t,i}) = \exp\left[-\frac{1}{R_k}(x_{i,k|k-1} - z_k)^2\right]. \quad (8)$$

251

where  $R_k$  is the observation error at time  $k$ , 0.01 m was set in this study;  $z_k$  represents the observed SD.

252

253

**Crossover mechanism:** The purpose of crossover operator is to exchange some genes for two or more chromosomes in a specified way, creating new individuals. GA mainly generates new individuals through this process, which determines the capability of global search. In this study, the arithmetic crossover method was used as the crossover operator to generate new individuals. Two particles were randomly selected from the resampled particle group and combined linearly to form a new particle. Assuming the two selected particles are  $\{x_m, x_n\}$ , the following equations were used to form the new particles:

254

255

256

257

258

259

260

$$x'_m = \alpha x_m + (1 - \beta) x_n. \quad (9)$$

261

262

$$x'_n = \beta x_n + (1 - \alpha) x_m. \quad (10)$$

263

where  $\alpha$ ,  $\beta$  are the empirical crossover coefficients, and  $\alpha = 0.45$ ,  $\beta = 0.55$  in this study. In order to ensure diversity among particles, newly formed particles will be discarded when the  $x'_m = x'_n$  occurred, and parent individuals will be re-selected from the particle group.

264

265

266

267

268

269

270

**Mutation mechanism:** The mutation in GA refers to replacing the gene values at some loci with other alleles to form a new individual. The mutation mechanism can be considered as a supplement to the crossover mechanism, which can increase the diversity of the population. Assuming that the randomly selected particle from the crossed particle set is  $x_k$ , the mutation operation is performed on the particle using the following equation:

271

272

273

274

275

276

277

$$x'_k = x_k + \eta * Uniform. \quad (11)$$

where *Uniform* refers a random number from a uniform distribution,  $\eta$  is an empirical coefficient, and 0.01 was set in this study.

It is noteworthy that a large number of particles may lead to filter collapse. In this study, we set the number of particles equal to 100 based on previous references (Mechri et al., 2014; Magnusson et al., 2017; Piazzini et al., 2018). Moreover, to prevent the particle ensemble from being unable to represent the prior model state due to structural deficiencies, a Gaussian-type model error,  $N(\mu, \sigma)$ , was added to the ensemble members. The  $\mu$  was obtained from the mean value of residual between

278 simulation and observation, and the variance  $\sigma$  was set to 0.01.

## 279 **2.4 DA experimental design**

### 280 **2.4.1 Perturbation of meteorological input data**

281 The accuracy of models' output largely depends on the input meteorological forcing dataset for  
282 land surface models, and meteorological forcing are one of the major sources of uncertainty affecting  
283 simulation results (Raleigh et al., 2015). The precipitation and air temperature are the most important  
284 input elements for snow simulations since their roles in determining the quantity of rainfall and  
285 snowfall.

286 To produce the forcing data ensemble, the air temperature and precipitation were perturbed  
287 following the method of Lei et al. (2014). In this study, the precipitation was assumed to have an error  
288 with a log-normal distribution, and it is expressed as follows:

$$289 \quad P_t^i = \exp(\mu_{\ln P} + \varphi_{P,i} \cdot \sigma_{\ln P} / 2). \quad (12)$$

$$290 \quad \sigma_{\ln P} = \sqrt{\ln \left( \frac{(\alpha_p \cdot P_t)^2}{P_t^2} + 1 \right)}. \quad (13)$$

$$291 \quad \mu_{\ln P} = \ln \left( \frac{P_t^2}{\sqrt{P_t^2 + (\alpha_p \cdot P_t)^2}} \right). \quad (14)$$

292 where  $P_t$  and  $P_t^i$  are the observed and perturbed precipitation at time  $t$ , respectively. The log  
293 transformation of  $P_t^i$  is a Gaussian distribution with a mean ( $\mu_{\ln P}$ ) and a standard deviation ( $\sigma_{\ln P}$ );  
294  $\alpha_p$  is the variance scaling factor of the precipitation, which was set to 0.5 in this study; and  $\varphi_{P,i}$  is  
295 a normally distributed random number. Meanwhile, the ensemble of the air temperature was obtained  
296 as follows:

$$297 \quad T_t^i = T_t - \gamma(1 - 2w^i), w^i \sim U(0,1). \quad (15)$$

298 Where  $T_t$  and  $T_t^i$  are the observed and perturbed air temperatures at time  $t$ , respectively;  $\gamma$   
299 is the variance scaling factor of the temperature with a value of 2.0; and  $w^i$  is the random noise with  
300 a uniform distribution between 0 and 1. A forcing ensemble containing 100 particles was obtained  
301 through above perturbation method in this study.

### 302 **2.4.2 Evaluation metrics**

303 In order to properly quantify the filter performance, each experiment is evaluated by statistical

304 analysis based on the daily mean values of simulations and observations. In this study, we used the  
 305 Kling-Gupta efficiency (KGE) coefficient (Gupta et al., 2009) to evaluate the filter performance,  
 306 which allows the analysis of how the assimilation of snow observations succeeds in properly updating  
 307 the model simulations, on average:

$$308 \quad KGE = 1 - \sqrt{(r-1)^2 + (a-1)^2 + (b-1)^2}. \quad (16)$$

309 where  $r$  is the linear correlation coefficient between the simulated and observed SD;  $a$  is the ratio  
 310 of the standard deviation of simulated SD to the standard deviation of the observed ones; and  $b$  is the  
 311 ratio of the mean of simulated SD to the mean of observed ones, here, the simulated SD is the mean  
 312 SD ensemble simulations. Theoretically, when  $r=1, a=1$  and  $b=1$  in Equation (16), the KGE  
 313 will obtain the optimal value which equals to 1, and this illustrates that the simulated SD highly  
 314 consistently with the observed ones.

315 The time series of SD obtained from assimilation scenarios was compared to observations for  
 316 evaluating the performance of the assimilation, and the root-mean-square error (RMSE) was  
 317 employed:

$$318 \quad RMSE = \sqrt{\frac{1}{N} \sum_{i=1}^N (obs(i) - sim(i))^2}. \quad (17)$$

319 where  $N$  is the total number of observations,  $sim(i)$  is the simulated value at time  $i$ , and  $obs(i)$   
 320 is the observed value at time  $i$ .

321 Another statistical index is the continuous ranked probability skill score (CRPSS), which is  
 322 evaluated to assess changes to the overall accuracy of the ensemble simulations of each experiment  
 323 (CRPS) by considering the open-loop ensemble control run as the reference one ( $CRPS_{ref}$ ), and the  
 324 calculation scheme is shown in the following formula:

$$325 \quad CRPSS = 1 - \frac{CRPS}{CRPS_{ref}}. \quad (18)$$

326 where CRPS is the continuous ranked probability score which can measure the difference between  
 327 continuous probability distribution and deterministic observation samples (detail in Hersbach, 2000).  
 328 A smaller CRPS value indicates better probabilistic simulation and the CRPS score of a perfect  
 329 simulation would equal to 0. Therefore, the changes in overall accuracy of the SD ensemble  
 330 simulations can be measured by CRPSS. However, unlike the CRPS score, the optimal CRPSS score  
 331 is equal to 1 and negative values indicate a negative improvement with respect to the reference control  
 332 run.

### 333 **3. Results and discussion**

### 334 3.1 Open-loop ensemble simulations

335 In order to investigate the impact of meteorological perturbations on snow simulations, an  
336 ensemble containing 100 SD simulations derived from as many different meteorological conditions  
337 was analyzed. For the sake of concision and clarity, we considered only one winter season for  
338 implementing snow simulation experiment at each site, and the results are shown in Figure 2. As  
339 shown in Figure 2, the possible overestimation and underestimation of SD simulations produced by  
340 the perturbation forcing data were contained within the ensemble spread, which is a direct  
341 consequence of the perturbation of the forcing data. Since the meteorological perturbations are  
342 unbiased, the physical processes with nonlinear characteristics within the model is supposed to be the  
343 main reason for the uncertainty (Piazzini et al. 2018). During the winter season in northern hemisphere,  
344 precipitation and air temperature are primary factors that can determine the total amount of snow.

345 As Figure 2 shows, the intervals of SD ensemble are significantly different at different sites,  
346 although an identical meteorological perturbation method was used. At some sites, such as ATY,  
347 MOHE, WFJ, and CDP, larger SD ensemble spreads were obtained, and most of the SD observations  
348 were covered by the ensemble spread. In this case, high-quality particles can be directly selected from  
349 the ensemble. However, at some other sites, such as ROPA, SDA, and SASP, narrow SD ensemble  
350 spreads were obtained, and the uncertainty interval of simulated SD can hardly cover the observations.  
351 In this case, the so-called high-quality particles cannot even be found in the ensemble, and the model  
352 prior error becomes a prerequisite for successful assimilation at this time. Especially at the ROPA site,  
353 the snow cover was extremely unstable, resulting in difficulty in figuring out any variation rules of  
354 SD. The narrow SD ensemble spread at this site also demonstrates that precipitation and air  
355 temperature were not the main factors causing snow change. According to the literature, sublimation  
356 losses at ROPA ranged from 24% to 33% of total annual ablation and occurred 60% of the time during  
357 which snow was present. A high sublimation rate may be the main reason for snow instability (Herrero  
358 et al., 2016; You et al., 2020a). This directly leads to a perfect ensemble spread that can cover all  
359 observations cannot be produced by perturbing the air temperature and precipitation. Generally  
360 speaking, the ensemble produced by perturbing air temperature and precipitation does not contain  
361 high-quality particles at this site. It was found that the spread of SD ensembles increases when a  
362 snowfall event occurs because the perturbation in precipitation would provide different input snow  
363 rates for model realization at all sites. Despite this, we still found that the simulated SD deviated  
364 significantly from the observation. For example, at SNQ site, the maximum value of simulated SD  
365 was almost half the maximum value of observed SD. In this case, it is impossible to obtain a simulated  
366 SD ensemble spread that can cover or nearly cover the observation through perturbing the  
367 meteorological forcing data. On the one hand, precipitation and air temperature are not the dominant  
368 factors affecting snow cover change, which leads to a narrowed ensemble spread at these sites. On  
369 the other hand, although the variation trend of snow cover can be accurately expressed by the Noah-

370 MP model, serious underestimation of the simulated SD shows that the snow simulation performance  
371 of Noah-MP is poor at these sites. Nonetheless, the simulated ensembles will be improved whenever  
372 the prior error of model state is considered.

### 373 *3.2 DA simulations with perturbed forcing data*

374 Generally, the ability of a model to simulate autonomously can be limited if observation data is  
375 assimilated too frequently, resulting in assimilation results that are essentially the same as the  
376 observations and do not reflect the differences among models. To address this, the site's SD  
377 measurements were assimilated into the Noah-MP model with an observation frequency of five days  
378 in this study, enabling the GPF to perform differently at distinct sites. Figure 3 shows the SD  
379 assimilation results across snow climates, indicating a substantial improvement in the SD simulations  
380 with satisfactory assimilation performance at all sites. The GPF algorithm can handle not only serious  
381 underestimations, such as at SNQ, SDA, but also overestimations during the snow ablation period, as  
382 seen at CDP, SASP, ATY, and MOHE sites. These results demonstrate the effectiveness of the GPF  
383 algorithm as a snow data assimilation scheme and its ability to significantly improve SD simulations,  
384 despite the numerous overestimations and underestimations that may occur in the Noah-MP model's  
385 snow simulation results across snow climates.

386 The effectiveness of GPF in updating SD simulations is demonstrated by the KGE values of the  
387 DA simulations with perturbed meteorological forcing data, as shown in Figure 4. Although the mean  
388 ensemble simulations of SD exhibit substantial improvement at all sites, not all ensemble members  
389 were improved, as per the distribution of GPF-DA KGE values. Some ensemble members achieved  
390 significant improvement at sites like SDA, SASP, MOHE, and SNQ, while others showed only slight  
391 improvement at sites like ATY, WFJ. Figure 4 also reveals that updating SD model simulations at  
392 ROPA and WFJ sites is more challenging. Snow simulation performance at the ROPA site is known  
393 to be poor due to the high sublimation rate. Certainly, the median value of SD ensemble prediction  
394 KGE values is expected to be below zero at this site, indicating that there are few qualified simulations  
395 in the prediction ensemble. While the GPF succeeds in enhancing the SD simulations at ROPA, the  
396 distribution of GPF-DA KGE values is not concentrated enough, with the 25th percentile  
397 approximately at 0.2 and the 75th percentile at about 0.7, indicating that the GPF assimilation  
398 algorithm cannot enhance all members but can raise the mean level and obtain an approximation of  
399 the optimal posterior estimation. Conversely, the assimilation of snow measurements at CDP site  
400 resulted in poor quality of the SD simulations compared to the open-loop ensemble simulations. The  
401 median value of GPF-DA KGE was lower than the median value of OL KGE, indicating that a  
402 considerable number of ensemble simulations failed to capture the observed values after assimilating  
403 snow measurements. However, Figure 3 shows that the mean ensemble simulations after assimilating  
404 snow measurements are much closer to SD observations. Thus, it underscores the importance of the  
405 ensemble mean in characterizing the filter effectiveness and the approximate value of the optimal

406 posterior estimation of model state. Additionally, the scale of the model ensemble spread was found  
407 to be the determinant factor that significantly affects assimilation results. A large ensemble spread  
408 can adjust the simulations toward the observed system state even if the model predictions are heavily  
409 biased.

410 Figure 5 displays the CRPSS value of GPF-DA at different sites. The smaller the CRPSS value,  
411 the worse the probabilistic simulation (with an optimal score of 1). The highest CRPSS score of 0.91  
412 was achieved at SASP, while the lowest score of 0.44 was observed at CDP. These results indicate  
413 that the GPF enhances the overall accuracy of ensemble simulations most at SASP and least at CDP  
414 with respect to the open-loop ensemble simulation. Certainly, this cannot be illustrated by the mean  
415 ensemble simulations (Figure 3) but is consistent with the KGE statistical results (Figure 4). Although  
416 the open-loop simulations at SNQ exhibited serious underestimation, a satisfactory assimilation result  
417 was obtained at this site with a CRPSS score of 0.87. At the SNQ site, the snow simulation  
418 performance of Noah-MP model is poor and the model shows serious underestimation during snow  
419 stable phase. Implementing a data assimilation experiment in this case is a tricky business since it is  
420 difficult to obtain a suitable simulated ensemble by perturbing the meteorological forcings. However,  
421 since the model prior error was considered in GPF algorithm, the overall accuracy of the ensemble  
422 simulations will be substantially enhanced and this is the reason why a satisfactory assimilation result  
423 at SNQ site can be obtained. ROPA was found to be a difficult site to enhance the overall accuracy of  
424 ensemble simulations, with a CRPSS score of only 0.58. The snow cover was highly unstable, and  
425 the variation of SD exhibited extreme irregularity, which may be the main obstacles to snow data  
426 assimilation at this site.

427 Based on these findings, we conclude that the effectiveness of GPF varied among snow climates:  
428 it can be employed as a snow data assimilation scheme across snow climates, however, its  
429 performance varied across different sites. It is necessary to explore the sensitivity of measurement  
430 frequency and ensemble size for the GPF assimilation scheme at various sites.

### 431 ***3.3 Sensitivity analysis of DA scheme to SD measurement frequency***

432 For complex land/snow process models, model errors can gradually lead to the system deviating  
433 from the true value. Therefore, it is necessary to continuously incorporate observations into the model  
434 framework to adjust the operating trajectory of the state. Obviously, the frequency of incorporating  
435 observations, that is, the assimilation interval, has an important impact on the assimilation system. To  
436 investigate the effect of the SD measurement frequency on the performance of GPF, we conducted a  
437 sensitivity experiment at eight sites. We aimed to determine how reducing the frequency of SD  
438 measurements affects the DA simulations. As expected, a decrease in SD measurement frequency led  
439 to a reduction in the impact of the GPF updating on the model simulations, resulting in a gradual  
440 increase in the mean RMSE value. Figure 6 illustrates the RMSE ensembles of SD simulations  
441 resulting from assimilating different frequency SD measurements over the snow period at each site.

442 Higher frequency SD assimilation improves the accuracy of the simulated SD, as shown by the lower  
443 RMSE value achieved when the frequency of SD measurement was set to five days. This means that  
444 more frequent SD measurements improve the accuracy of the model, which is particularly useful in  
445 regions where snow conditions can change rapidly. The range of RMSE values at different sites varied  
446 significantly, as it was related to the maximum value of SD. For instance, a thick snow at SNQ and  
447 WFJ sites during the snow period led to larger RMSEs of SD simulations. Notably, an increase in the  
448 length of the assimilation window generally resulted in a significant increase in the RMSE value.  
449 However, an abnormal occurrence was observed at the SDA site, where the assimilation effect of 20  
450 days of SD measurements was significantly better than that of 15 days. Although the RMSE  
451 distribution of SD assimilation results with 20 days of observations appeared superior to that of 15  
452 days, the RMSE mean values of the two were very close: 0.08 m and 0.07 m, respectively. Therefore,  
453 this anomaly can be ignored. These results indicate that the frequency of SD observations has a  
454 significant impact on the effectiveness of the GPF algorithm and that a dense amount of observational  
455 data can effectively improve the assimilation results.

### 456 ***3.4 Sensitivity analysis of DA scheme to ensemble size***

457 The results of the experiment aimed at evaluating the impact of particle number on the  
458 assimilation performance of GPF are presented in Figure 7. As expected, increasing the particle  
459 number up to the threshold leads to a significant improvement in the percent effective sample size.  
460 However, the filter performance does not improve significantly when the particle number exceeds the  
461 threshold. Figure 7 shows that the GPF algorithm yields the minimum error at all sites when the  
462 particle number is set to 100, indicating that one hundred particles can optimize the performance of  
463 the GPF algorithm. Although a large particle number can enhance particle diversity and prevent filter  
464 divergence, it increases the computation burden without reducing the system error. As illustrated in  
465 Figure 7, the RMSEs are generally at the same level when the particle number equals 120 and 160,  
466 and they are significantly larger than the RMSE when the particle number is equal to 100. The slight  
467 impact of the change in the particle number on the performance of GPF, when the particle number is  
468 below the threshold, indicates low system sensitivity to the ensemble size, and this is observed at all  
469 sites. Essentially, blindly increasing the particle number does not guarantee a better DA performance  
470 of the GPF algorithm. As demonstrated in Figure 7, the RMSEs of simulated snow-depth are virtually  
471 unchanged at all sites, despite an increase in the particle number from 120 to 160. This suggests that  
472 blindly increasing the ensemble size only increases the computational burden without improving the  
473 performance of the GPF.

### 474 ***3.5 Compared to traditional resampling methods***

475 To demonstrate the effectiveness of using genetic algorithms for particle resampling, we  
476 compared the results of our genetic algorithm (PF-G) to those of traditional resampling methods:

477 systematic resampling (PF-S) and multinomial resampling (PF-M), which are both commonly used  
478 in particle resampling. The calculation process for these methods is detailed in the particle filter  
479 introduction references. Figure 8 shows the RMSE values for SD simulations obtained using these  
480 three methods. We found that the PF-G outperforms PF-M and PF-S at all sites, as evidenced by the  
481 significantly smaller mean and median RMSE values. This indicates that the PF-G is suitable for  
482 snow data assimilation in various snow climates and is somewhat superior to traditional particle filters.  
483 At most sites (MOHE, ATY, SDA, and ROPA), PF-M and PF-S showed similar performance, meaning  
484 that these methods did not produce a significant difference in the assimilation results. This is because  
485 these traditional resampling methods can only mitigate particle degeneration by resampling particles,  
486 but are unable to prevent particle impoverishment. Therefore, they are unable to select high-quality  
487 particles and keep the particles have variety. Significantly, the mean and median RMSE values for  
488 PF-G were lower than those of PF-M and PF-S at several sites (SASP, SNQ, and WFJ) where the  
489 snow cover was relatively thick, with maximum SD during the snow period reaching 2.45 m, 2.95 m,  
490 and 2.40 m, respectively. This suggests that PF-G performs better in assimilating data from thick  
491 snow covers.

492 The multinomial and systematic resampling methods select particles from the original particle  
493 set at different levels or based on the accumulation of particle weights. Both of the resampling  
494 methods extract particles from the entire particle set, and the corresponding particle values do not  
495 undergo any essential changes. However, when compared to the two traditional particle resampling  
496 methods, the genetic algorithm first uses the fitness function to calculate the "survival rate" of each  
497 particle one by one, and then performs crossover, mutation and other operations on the selected  
498 particles. This approach ensures that the resampled particles are high-quality particles, which is the  
499 main reason why genetic particle filtering has an advantage in the snow data assimilation experiments.  
500 As Figure 8 shows, the assimilation error of the genetic particle filter is the smallest at all sites. From  
501 the results of the real assimilation experiment, it can be seen that genetic particle filtering has more  
502 advantages over the other two methods.

## 503 **4. Conclusions**

504 In this study, we investigated the potential of using GPF as a snow data assimilation scheme  
505 across eight sites with varying snow climates. We addressed the problem of degeneration and  
506 impoverishment in PF algorithm by using the genetic algorithm to resample particles. We also  
507 examined the sensitivity of GPF scheme to measurement frequency and ensemble size. The main  
508 findings of this study are as follows:

- 509 1. The GPF was an effective snow data assimilation scheme and can be used across different snow  
510 climates. The genetic algorithm effectively addressed the problem of particle degeneration and



511 impoverishment in the PF algorithm.

512 2. Our experiment showed that the system has low sensitivity to the particle number, and 100  
513 particles can achieve a better assimilation result across different snow climates. This indicates  
514 that 100 particles are suitable for representing the high dimensionality of the system.

515 3. We found that perturbations in meteorological forcing data were not sufficient to provide  
516 ensemble spread, resulting in poor filter performance. Particle inflation can make up for this  
517 deficiency. Moreover, we observed that the RMSE of simulated SD decreased significantly with  
518 the increase of the frequency of SD measurement, indicating that dense observational data can  
519 improve the assimilation results.

520 4. Compared to the two classic resampling methods, the particle filter with genetic algorithm as  
521 resampling method shows a better assimilation performance especially in a thick snow cover, the  
522 distributed RMSEs are more centralized and a smaller mean error will be obtained.

523 Our experiments were based on forcing data and snow observations from various sites with different  
524 snow climates. While our results provide a reference for applying GPF to snow data assimilation,  
525 further research is needed to investigate the performance of GPF on a regional scale and to explore  
526 the assimilation of snow observational data from remote sensing or wireless sensor networks into  
527 land surface models using GPF. In summary, our study demonstrates the feasibility of using GPF for  
528 snow data assimilation and provides valuable insights for future research in this area.

## 529 **Acknowledgements**

530 Our research received support from several sources, including the National Natural Science  
531 Foundation of China (grant number 42101361, 42130113, 41871251, and 41971326), the Scientific  
532 research project of higher education institutions in Anhui province, and the Key Research and  
533 Development Program of Anhui Province (2022107020028).

## 534 **References**

- 535 Abbasnezhadi, K., Rousseau, A. N., Foulon, E., and Savary, S.: Verification of regional deterministic  
536 precipitation analysis products using snow data assimilation for application in meteorological  
537 network assessment in sparsely gauged Nordic basins, *Journal of Hydrometeorology*, 22, 859-  
538 876, <https://doi.org/10.1175/JHM-D-20-0106.1>, 2021.
- 539 Abbaszadeh, P., Moradkhani, H., Yan, H. X.: Enhancing hydrologic data assimilation by evolutionary  
540 particle filter and Markov Chain Monte Carlo, *Advances in Water Resources*, 111, 192-204,  
541 <https://doi.org/10.1016/j.advwatres.2017.11.011>, 2018.
- 542 Ahmadi, M., Mojallali, H., Izadi-Zamanabadi, R.: State estimation of nonlinear stochastic systems  
543 using a novel meta-heuristic particle filter, *Swarm and Evolutionary Computation*, 4, 44-53,  
544 <https://doi.org/10.1016/j.swevo.2011.11.004>, 2012.

- 545 Andreadis, K. M., Lettenmaier, D. P.: Assimilating remotely sensed snow observations into a  
546 macroscale hydrology model, *Advances in water resources*, 29, 872-886, [https://doi.org/](https://doi.org/10.1016/j.advwatres.2005.08.004)  
547 10.1016/j.advwatres.2005.08.004, 2006.
- 548 Barnett, T. P., Adam, J. C., Lettenmaier, D. P.: Potential impacts of a warming climate on water  
549 availability in snow-dominated regions, *Nature*, 438, 303-309, [https://doi.org/](https://doi.org/10.1038/nature04141)  
550 10.1038/nature04141, 2005.
- 551 Balsamo, G., Albergel, C., Beljaars, A., Boussetta, S., Burun, E., Cloke, H., Dee, D., Dutra, E.,  
552 Munoz-Sabater, J., Pappenberger, F., de Rosnay, P., Stockdale, T., and Vitart, F.: ERA-  
553 Interim/Land: a global land surface reanalysis data set, *Hydrology and Earth System Sciences*,  
554 19, 389-407, <https://doi.org/10.5194/hess-19-389-2015>, 2015.
- 555 Bergeron, J. M., Trudel, M., Leconte, R.: Combined assimilation of streamflow and snow water  
556 equivalent for mid-term ensemble streamflow forecasts in snow-dominated regions, *Hydrology*  
557 *and Earth System Sciences*, 20, 4375-4389, <https://doi.org/10.5194/hess-20-4375-2016>, 2016.
- 558 Che, T., Li, X., Jin, R., and Huang, C. L.: Assimilating passive microwave remote sensing data into a  
559 land surface model to improve the estimation of snow depth, *Remote Sensing of Environment*,  
560 143, 54-63, <https://doi.org/10.1016/j.rse.2013.12.009>, 2014.
- 561 Chen, Z.: Bayesian filtering: From Kalman filters to particle filters, and beyond, *Adaptive Systems*  
562 *Laboratory Technical Report*, McMaster University, Hamilton, 25pp., 2003.
- 563 Chen, Y. Y., Yang, K., He, J., Qin, J., Shi, J. C., Du, J. Y., and He, Q.: Improving land surface  
564 temperature modeling for dry land of China, *Journal of Geophysical Research-Atmospheres*,  
565 116, D20104, <https://doi.org/10.1029/2011JD015921>, 2011.
- 566 Cortes, G., Giroto, M., Margulis, S.: Snow process estimation over the extratropical Andes using a  
567 data assimilation framework integrating MERRA data and Landsat imagery, *Water Resources*  
568 *Research*, 52, 2582-2600, <https://doi.org/10.1002/2015WR018376>, 2016.
- 569 Dee, D. P., Uppala, S. M., Simmons, A. J., Berrisford, P., Poli, P., Kobayashi, S., Andrae, U.,  
570 Balmaseda, M. A., Balsamo, G., Bauer, P., Bechtold, P., Beljaars, A. C. M., van de Berg, L.,  
571 Bidlot, J., Bormann, N., Delsol, C., Dragani, R., Fuentes, M., Geer, A. J., Haimberger, L., Healy,  
572 S. B., Hersbach, H., Holm, E. V., Isaksen, L., Kallberg, P., Koehler, M., Matricardi, M., McNally,  
573 A. P., Monge-Sanz, B. M., Morcrette, J. J., Park, B. -K., Peubey, C., de Rosnay, P., Tavolato, C.,  
574 Thepaut, J. N., and Vitart, F.: The ERA-Interim reanalysis: configuration and performance of the  
575 data assimilation system, *Quarterly Journal of the Royal Meteorological Society*, 137, 553-597,  
576 <https://doi.org/10.1002/qj.828>, 2011.
- 577 Dechant, C., Moradkhani, H.: Radiance data assimilation for operational snow and streamflow  
578 forecasting, *Advances in Water Resources*, 34, 351-364, [https://doi.org/](https://doi.org/10.1016/j.advwatres.2010.12.009)  
579 10.1016/j.advwatres.2010.12.009, 2011.
- 580 Deschamps-Berger, C., Cluzet, B., Dumont, M., Lafaysse, M., Berthier, E., Fanise, P., Gascoin, S.:  
581 Improving the Spatial Distribution of Snow Cover Simulations by Assimilation of Satellite  
582 Stereoscopic Imagery, *Water Resources Research*, 58, <https://doi.org/10.1029/2021WR030271>,  
583 2022.
- 584 Dettinger, M.: Climate change impacts in the third dimension, *Nature Geoscience*, 7, 166-167,

585 <https://doi.org/10.1038/ngeo2096>, 2014.

586 Evensen, G.: The ensemble Kalman filter: Theoretical formulation and practical implementation,  
587 *Ocean Dynamics*, 53, 343-367, <https://doi.org/10.1007/s10236-003-0036-9>, 2003.

588 Gelb, A.: Optimal linear filtering, in: Applied optimal estimation, MIT Press, Cambridge, Mass, 102-  
589 155, 1974.

590 Gordon, N. J., Salmond, D. J., Smith, A. F. M.: Novel-Approach to nonlinear non-Gaussian bayesian  
591 state estimation, *IEE Proceedings-F Radar and Signal Processing*, 140, 107-113, <https://doi.org/10.1049/ip-f-2.1993.0015>, 1993.

593 Griessinger, N., Seibert, J., Magnusson, J., and Jonas, T.: Assessing the benefit of snow data  
594 assimilation for runoff modeling in Alpine catchments, *Hydrology and Earth System Sciences*,  
595 20, 3895-3905, <https://doi.org/10.5194/hess-20-3895-2016>, 2016.

596 Gupta, H. V., Kling, H., Yilmaz, K. K., and Martinez, G. F.: Decomposition of the mean squared error  
597 and NSE performance criteria: Implications for improving hydrological modelling, *Journal of*  
598 *Hydrology*, 377, 80-91, <https://doi.org/10.5194/10.1016/j.jhydrol.2009.08.003>, 2009.

599 Herrero, J., Polo, M. J., Monino, A., and Losada, M. A.: An energy balance snowmelt model in a  
600 Mediterranean site, *Journal of Hydrology*, 371, 98-107, <https://doi.org/10.1016/j.jhydrol.2009.03.021>, 2009.

602 Herrero, J., Polo, M. J., Pimentel, R., and Pérez-Palazón, M. J.: Meteorology and snow depth at  
603 Refugio Poqueira (Sierra Nevada, Spain) at 2510 m 2008-2015, PANGEA, 2016.

604 Hersbach, H.: Decomposition of the continuous ranked probability score for ensemble prediction  
605 systems, *Weather and Forecasting*, 15, 559-570, [https://doi.org/10.1175/1520-0434\(2000\)015<0559:DOTCRP>2.0.CO;2](https://doi.org/10.1175/1520-0434(2000)015<0559:DOTCRP>2.0.CO;2), 2000.

607 Kwok, N., Fang, G., Zhou, W.: Evolutionary particle filter: resampling from the genetic algorithm  
608 perspective. In: *Proceedings of International Conference on Intelligent Robots and Systems*,  
609 Shaw Conference Centre, Edmonton, Alberta, Canada, August 2-6, pp. 2935-2940, 2005.

610 Kwon, Y., Yang, Z. L., Hoar, T. J., and Toure, A. M.: Improving the radiance assimilation performance  
611 in estimating snow water storage across snow and land-cover types in North America, *Journal*  
612 *of Hydrometeorology*, 18, 651-668, <https://doi.org/10.1175/JHM-D-16-0102.1>, 2017.

613 Lei, F. N., Huang, C. L., Shen, H. F., and Li, X.: Improving the estimation of hydrological states in  
614 the SWAT model via the ensemble Kalman smoother: Synthetic experiments for the Heihe River  
615 Basin in northwest China, *Advances in Water Resources*, 67, 32-45, <https://doi.org/10.1016/j.advwatres.2014.02.008>, 2014.

617 Malik, M. J., van der Velde, R., Vekerdy, Z., and Su, Z. B.: Assimilation of Satellite-Observed Snow  
618 Albedo in a Land Surface Model, *Journal of Hydrometeorology*, 13, 1119-1130, <https://doi.org/10.1175/JHM-D-11-0125.1>, 2012.

620 Magnusson, J., Gustafsson, D., Husler, F., and Jonas, T.: Assimilation of point SWE data into a  
621 distributed snow cover model comparing two contrasting methods, *Water Resources Research*,  
622 50, 7816-7835, <https://doi.org/10.1002/2014WR015302>, 2014.

- 623 Margulis, S. A., Giroto, M., Cortes, G., and Durand, M.: A particle batch smoother approach to snow  
624 water equivalent estimation, *Journal of Hydrometeorology*, 16, 1752-1772, [https://doi.org/](https://doi.org/10.1175/JHM-D-14-0177.1)  
625 10.1175/JHM-D-14-0177.1, 2015.
- 626 Magnusson, J., Winstral, A., Stordal, A. S., Essery, R., and Jonas, T: Improving physically based snow  
627 simulations by assimilating snow depths using the particle filter, *Water Resources Research*, 53,  
628 1125-1143, <https://doi.org/10.1002/2016WR019092>, 2017.
- 629 Moradkhani, H., Hsu, K. L., Gupta, H., and Sorooshian, S.: Uncertainty assessment of hydrologic  
630 model states and parameters: Sequential data assimilation using the particle filter, *Water*  
631 *Resources Research*, 41, W05012, <https://doi.org/10.1029/2004WR003604>, 2005.
- 632 Mechri, R., Otle, C., Pannekoucke, O., and Kallel, A.: Genetic particle filter application to land  
633 surface temperature downscaling, *Journal of Geophysical Research-Atmospheres*, 119, 2131-  
634 2146, <https://doi.org/10.1002/2013JD020354>, 2014.
- 635 Niu, G. Y., Yang, Z. L.: Effects of vegetation canopy processes on snow surface energy and mass  
636 balances, *Journal of Geophysical Research-Atmospheres*, 109, D23111, [https://doi.org/](https://doi.org/10.1029/2004JD004884)  
637 10.1029/2004JD004884, 2004.
- 638 Niu, G. Y., Yang, Z. L.: Effects of frozen soil on snowmelt runoff and soil water storage at a  
639 continental scale, *Journal of Hydrometeorology*, 7, 937-952, <https://doi.org/10.1175/JHM538.1>,  
640 2006.
- 641 Oaida, C. M., Reager, J. T., Andreadis, K. M., David, C. H., Levoe, S. R., Painter, T. H., Bormann, K.  
642 J., Trangsrud, A. R., Giroto, M., and Famiglietti, J. S.: A high-resolution data assimilation  
643 framework for snow water equivalent estimation across the western United States and validation  
644 with the airborne snow observatory, *Journal of Hydrometeorology*, 20, 357-378,  
645 <https://doi.org/10.1175/JHM-D-18-0009.1>, 2019.
- 646 Park, S., Hwang, J. P., Kim, E., and Kang, H. J.: A new evolutionary particle filter for the prevention  
647 of sample impoverishment, *IEEE Transaction on Evolutionary Computation*, 13, 801-809,  
648 <https://doi.org/10.1109/TEVC.2008.2011729>, 2009.
- 649 Parrish, M. A., Moradkhani, H., DeChant, C. M.: Toward reduction of model uncertainty: Integration  
650 of Bayesian model averaging and data assimilation, *Water Resources Research*, 48, W03519,  
651 <https://doi.org/10.1029/2011WR011116>, 2012.
- 652 Piazzzi, G., Campo, L., Gabellani, S., Castelli, F., Cremonese, E., di Cella, U. M., Stevenin, H., and  
653 Ratto, S. M.: An EnKF-based scheme for snow multivariable data assimilation at an Alpine site,  
654 *Journal of Hydrology and Hydromechanics*, 67, 4-19, <https://doi.org/10.2478/joh-h-2018-0013>,  
655 2019.
- 656 Piazzzi, G., Thirel, G., Campo, L., and Gabellani, S.: A particle filter scheme for multivariate data  
657 assimilation into a point-scale snowpack model in an Alpine environment, *Cryosphere*, 12, 2287-  
658 2306, <https://doi.org/10.5194/tc-12-2287-2018>, 2018.
- 659 Pulliainen, J., Luojus, K., Derksen, C., Mudryk, L., Lemmetyinen, J., Salminen, M., Ikonen, J., Takala,  
660 M., Cohen, J., Smolander, T., and Norberg, J.: Patterns and trends of Northern Hemisphere snow  
661 mass from 1980 to 2018, *Nature*, 581, 294-298, <https://doi.org/10.1038/s41586-020-2258-0>,  
662 2020.

- 663 Rautiainen, K., Lemmetyinen J., Schwank, M., Kontu, A., Menard, C. B., Matzler, C., Drusch, M.,  
664 Wiesmann, A., Ikonen, J., and Pulliainen, J.: Detection of soil freezing from L-band passive  
665 microwave observations, *Remote Sensing of Environment*, 147, 206-218, <https://doi.org/10.1016/j.rse.2014.03.007>, 2014.
- 667 Raleigh, M. S., Lundquist, J. D., Clark, M.P.: Exploring the impact of forcing error characteristics on  
668 physically based snow simulations within a global sensitivity analysis framework, *Hydrology  
669 and Earth System Sciences*, 19, 3153-3179, <https://doi.org/10.5194/hess-19-3153-2015>, 2015.
- 670 Rings, J., Vrugt, J. A., Schoups, G., Huisman, J. A., and Vereecken, H.: Bayesian model averaging  
671 using particle filtering and Gaussian mixture modeling: Theory, concepts, and simulation  
672 experiments, *Water Resources Research*, 48, W05520, <https://doi.org/10.1029/2011WR011607>,  
673 2012.
- 674 Smyth, E. J., Raleigh, M. S., Small, E. E.: Improving SWE estimation with data assimilation: the  
675 influence of snow depth observation timing and uncertainty, *Water Resources Research*, 56,  
676 e2019WR026853, <https://doi.org/10.1029/2019WR026853>, 2020.
- 677 Sturm, M., Holmgren, J., Liston, G. E.: A seasonal snow cover classification system for local to global  
678 applications, *Journal of Climate*, 8, 1261-1283, [https://doi.org/10.1175/1520-0442\(1995\)008<1  
679 261:ASSCCS>2.0.CO;2](https://doi.org/10.1175/1520-0442(1995)008<1261:ASSCCS>2.0.CO;2), 1995.
- 680 Su, H., Yang, Z. L., Niu, G. Y., and Dickinson, R. E.: Enhancing the estimation of continental-scale  
681 snow water equivalent by assimilating MODIS snow cover with the ensemble Kalman filter,  
682 *Journal of Geophysical Research-Atmospheres*, 113, D08120, [https://doi.org/10.1029/2007JD00  
683 9232](https://doi.org/10.1029/2007JD009232), 2008.
- 684 Snyder, C.: Particle filters, the optimal proposal and high-dimensional systems, *ECMWF Seminar on  
685 Data Assimilation for Atmosphere and Ocean*, pp. 6-9, Reading, U. K., 2011.
- 686 Takala, M., Luoju, K., Pulliainen, J., Derksen, C., Lemmetyinen, J., Karna, J. P., Koskinen, J., and  
687 Bojkov, B.: Estimating northern hemisphere snow water equivalent for climate research through  
688 assimilation of space-borne radiometer data and ground-based measurements, *Remote Sensing  
689 of Environment*, 115, 3517-3529, <https://doi.org/10.1016/j.rse.2011.08.014>, 2011.
- 690 Trujillo, E., Molotch, N.P.: Snowpack regimes of the Western United States, *Water Resources  
691 Research*, 50, 5611-5623, <https://doi.org/10.1002/2013WR014753>, 2014.
- 692 Van Leeuwen, P. J.: Nonlinear data assimilation in geosciences: An extremely efficient particle filter,  
693 *Quarterly Journal of the Royal Meteorological Society*, 136, 1991-1999, [https://doi.org/  
694 10.1002/qj.699](https://doi.org/10.1002/qj.699), 2010.
- 695 Wayand, N. E., Massmann, A., Butler, C., Keenan, E., Stemberis, J., and Lundquist, J. D.: A  
696 meteorological and snow observational data set from Snoqualmie Pass (921 m), Washington  
697 Cascades, USA, *Water Resources Research*, 51, 10092-10103, [https://doi.org/10.1002/2015WR  
698 017773](https://doi.org/10.1002/2015WR017773), 2015.
- 699 Weerts, A. H., El Serafy, G. Y. H.: Particle filtering and ensemble Kalman filtering for state updating  
700 with hydrological conceptual rainfall-runoff models, *Water Resources Research*, 42, W09403,  
701 <https://doi.org/10.1029/2005WR004093>, 2006.

702 Wever, N., Schmid, L., Heilig, A., Eisen, O., Fierz, C., and Lehning, M.: Verification of the multi-  
703 layer SNOWPACK model with different water transport schemes, *The Cryosphere*, 9, 2271-  
704 2293, <https://doi.org/10.5194/tc-9-2271-2015>, 2015.

705 Yang, J. M., Li, C. Z.: Assimilation of D-InSAR snow depth data by an ensemble Kalman filter,  
706 *Arabian Journal of Geosciences*, 14, 1-14, <https://doi.org/10.1007/s12517-021-06699-y>, 2021.

707 You, Y. H., Huang, C. L., Yang, Z. L., Zhang, Y., Bai, Y. L., and Gu, J.: Assessing Noah-MP  
708 parameterization sensitivity and uncertainty interval across snow climates, *Journal of*  
709 *Geophysical Research-Atmospheres*, 125, e2019JD030417, [https://doi.org/10.1029/2019JD030](https://doi.org/10.1029/2019JD030417)  
710 417, 2020.

711 Zhang, T. J.: Influence of the seasonal snow cover on the ground thermal regime: An overview,  
712 *Reviews of Geophysics*, 43, RG4002, <https://doi.org/10.1029/2004RG000157>, 2005.

713 Zhu, G. F., Li, X., Ma, J.Z., Wang, Y. Q., Liu, S. M., Huang, C. L., Zhang, K., and Hu, X. L.: A new  
714 moving strategy for the sequential Monte Carlo approach in optimizing the hydrological model  
715 parameters, *Advances in Water Resources*, 114, 164-179, [https://doi.org/10.1016/j.advwatres.](https://doi.org/10.1016/j.advwatres.2018.02.007)  
716 2018.02.007, 2018.

717

718

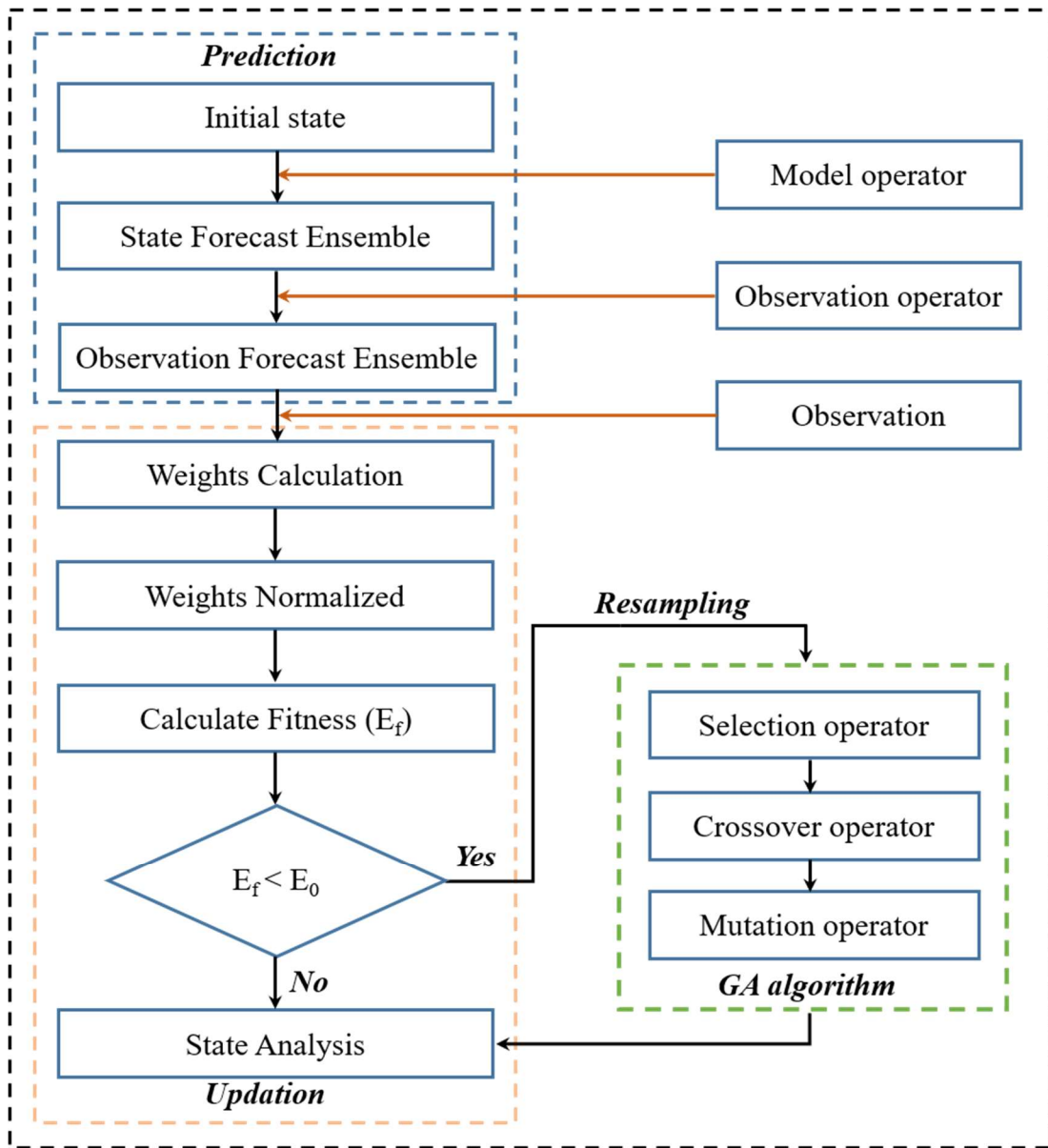


**Figure 1.** Flowchart of Genetic particle filter

719

720

721

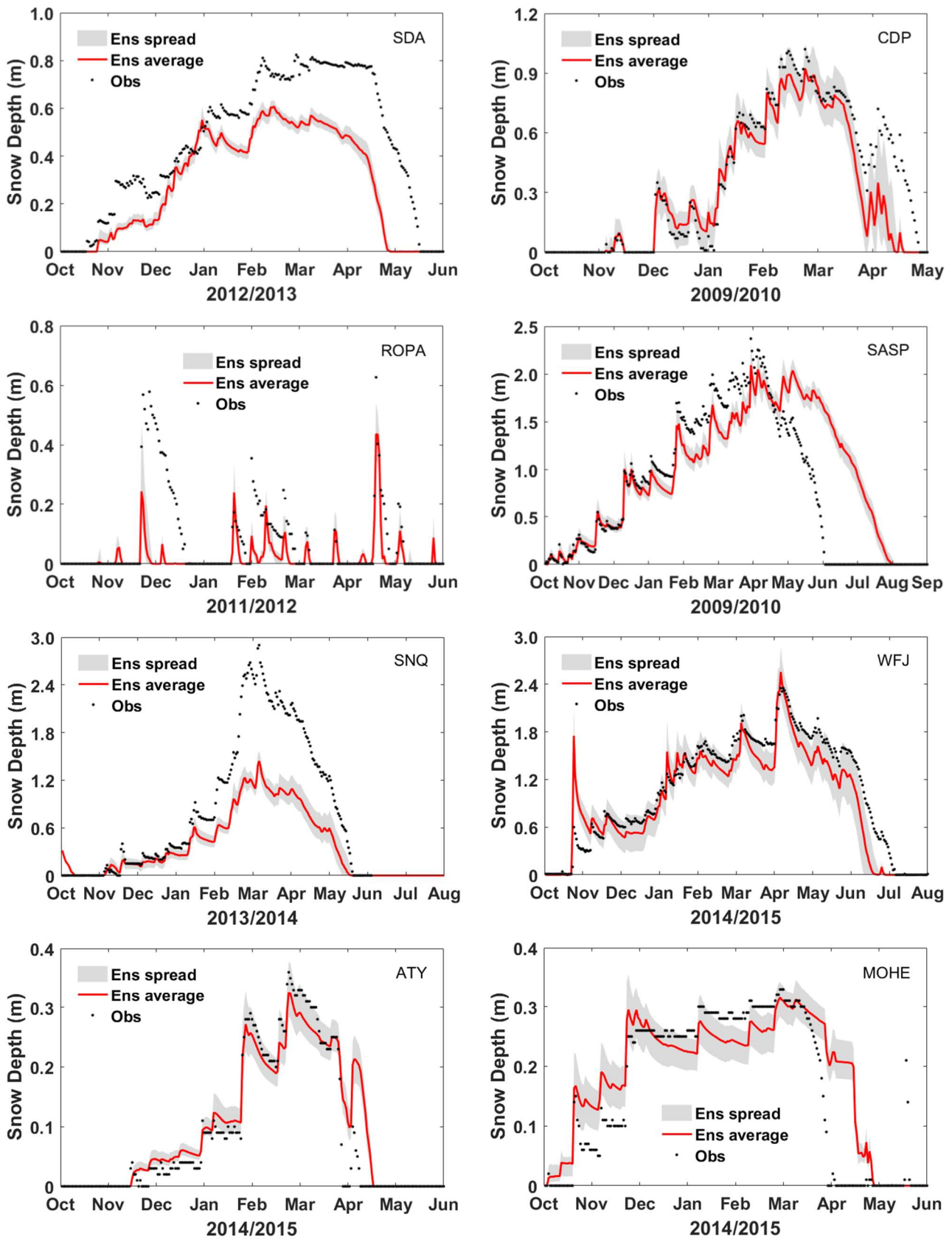


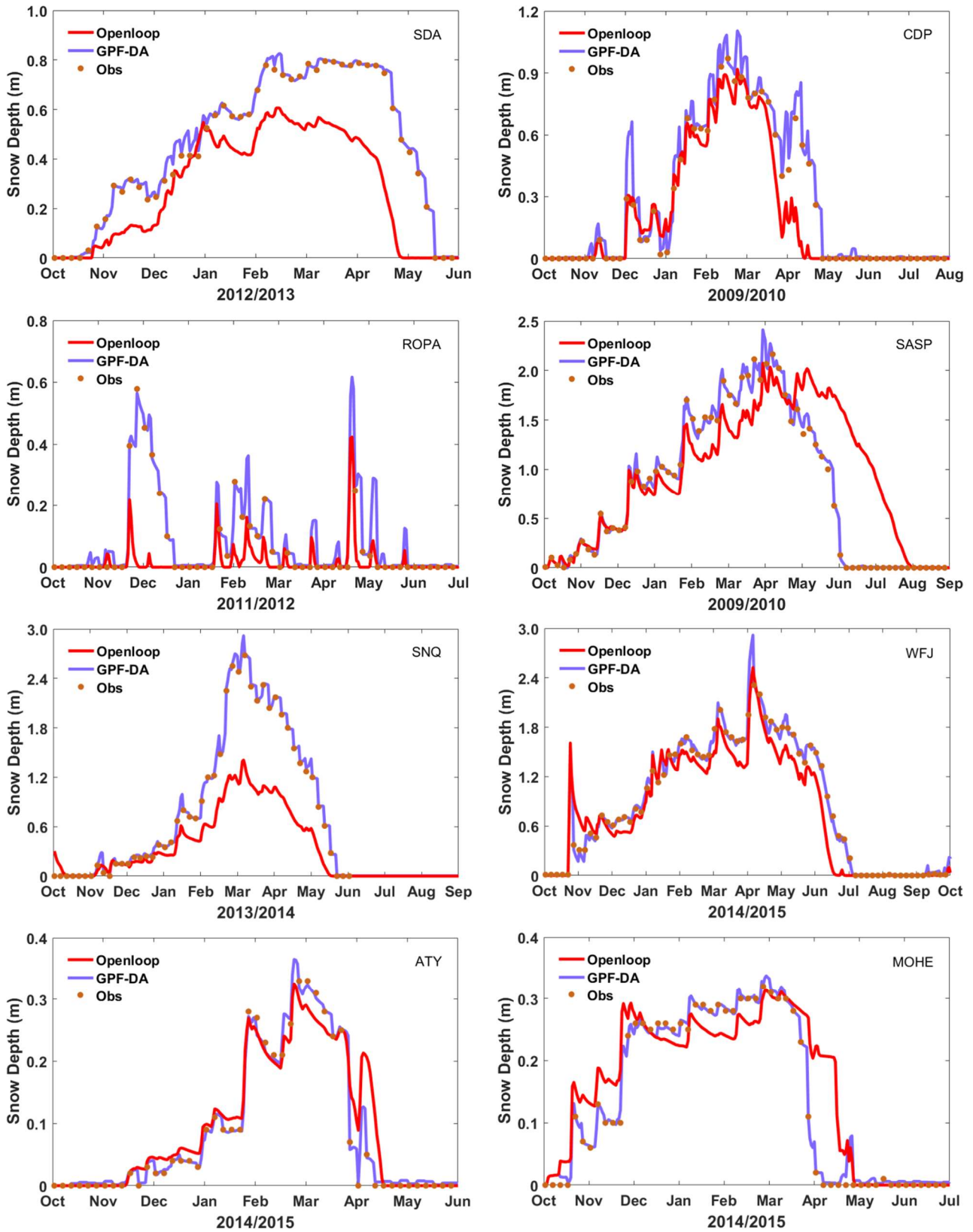
**Figure 2.** Impact of the meteorological uncertainty on snow depth ensemble simulations

722

723

724





725

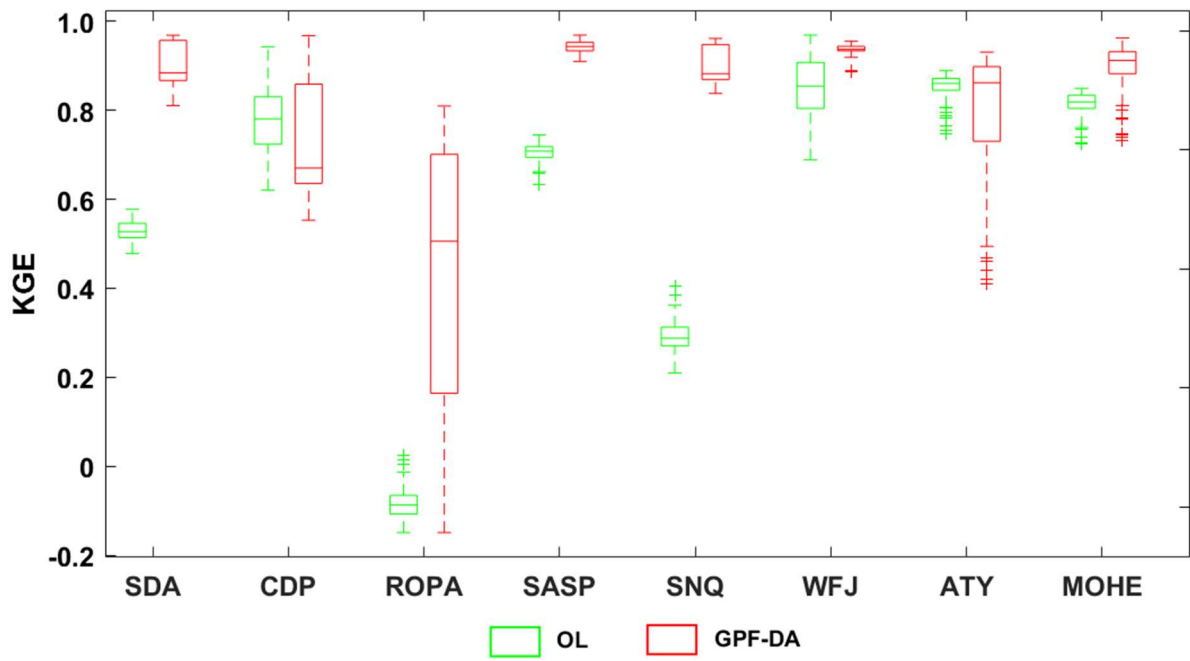
726

**Figure 3.** Evaluation of the SD at eight sites from mean ensemble simulation and assimilation with the measurements.

727

728

729

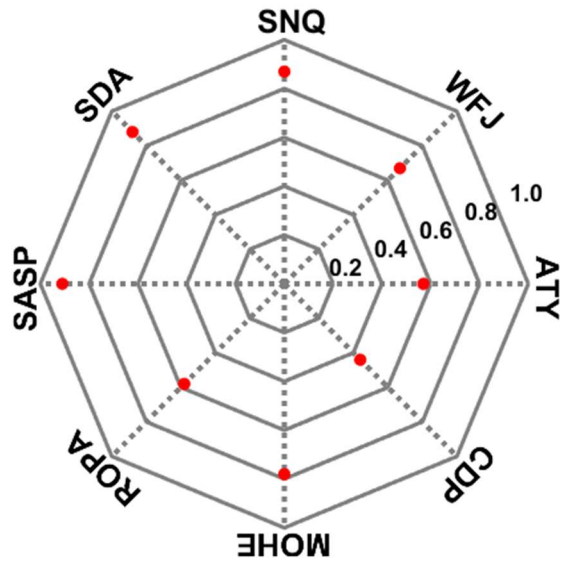


730

731 **Figure 4.** The KGE values of SD simulations, the OL and GPF-DA are in green, red, respectively.

732 The bottom and top edges of each box indicate the 25th 75th percentiles, respectively. The line in the  
 733 middle of each box is the median.

734

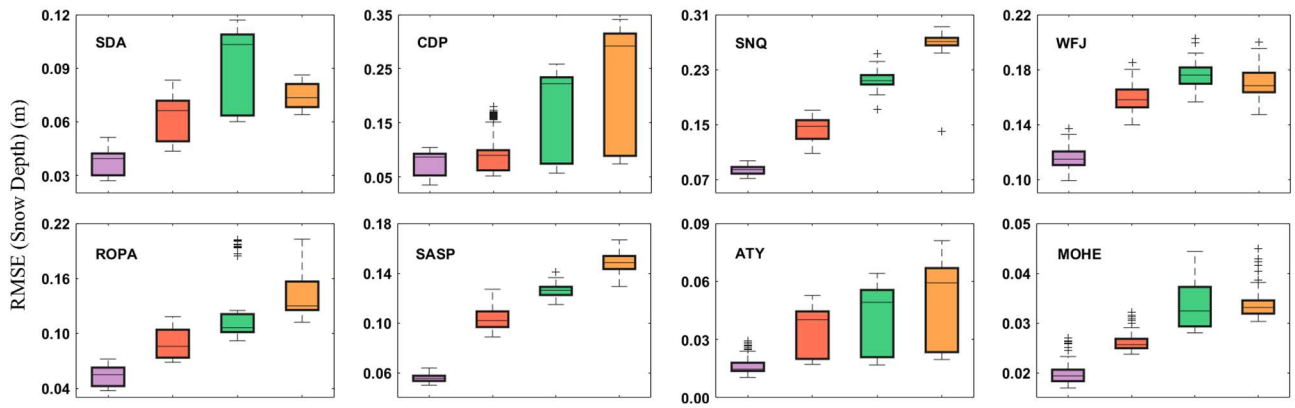


735

736

**Figure 5.** Comparison of the CRPSS value of GPF-DA at different sites.

737



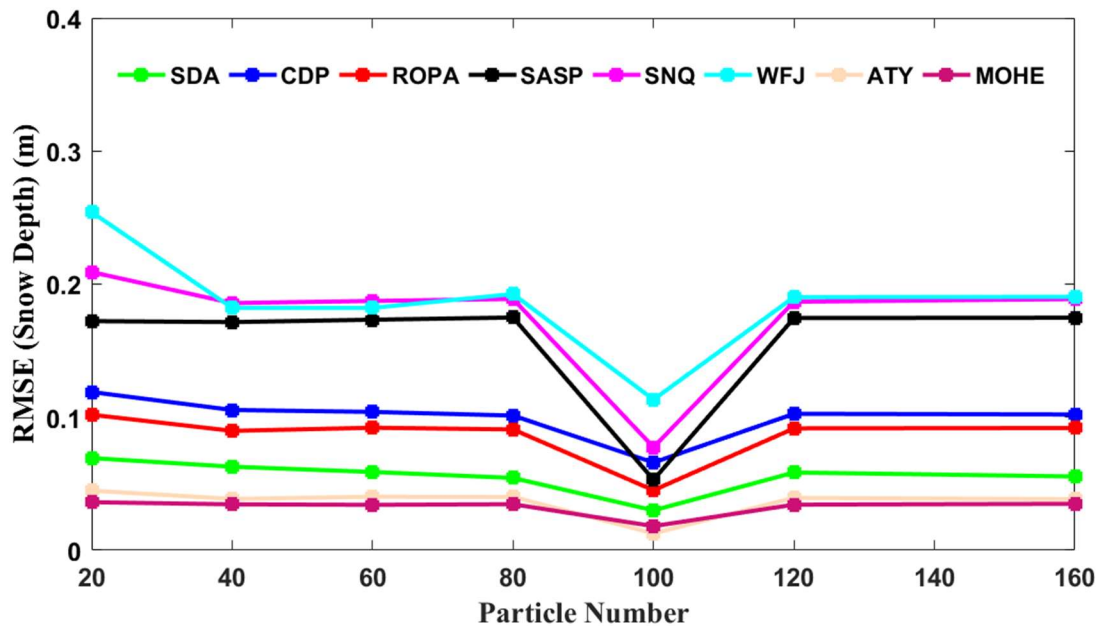
738

739

740

741

**Figure 6.** The RMSE values of SD simulations at different sites, from left to right in each subfigure are the assimilation observation frequency is 5, 10, 15, 20 days, respectively, and with different colors.

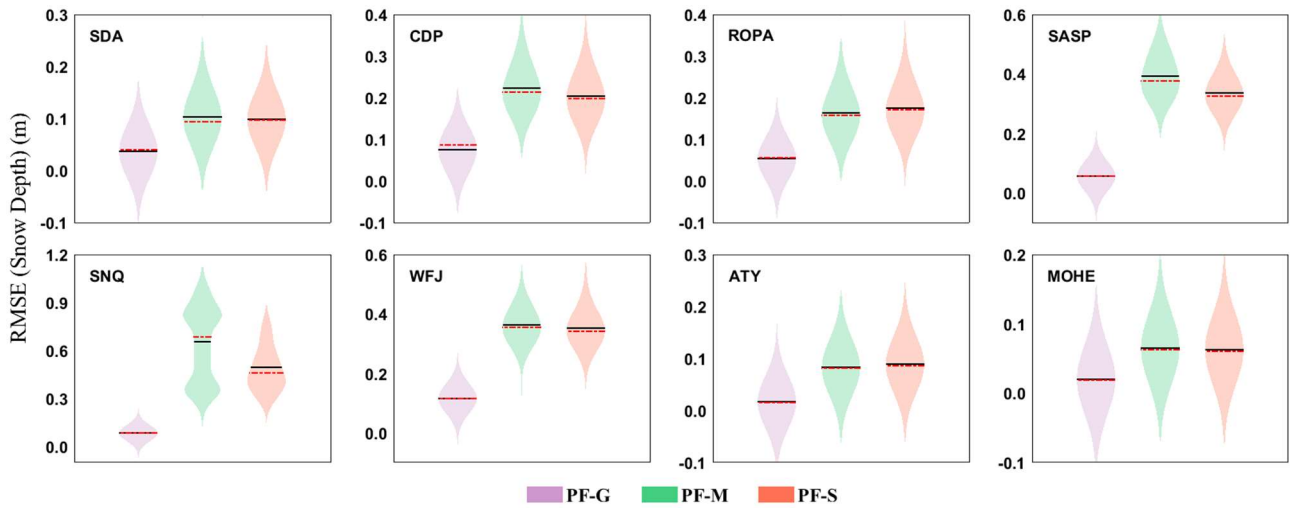


742

743 **Figure 7.** Sensitivity analysis of the GPF snow DA scheme to particle number at eight sites, during

744 different snow periods.

745



746

747 **Figure 8.** The RMSE values of SD simulations by three different resampling methods. For each  
 748 subfigure, from left to right are the particles resampled by genetic algorithm, multinomial method,  
 749 systematic method, respectively, and with different colors, the black line indicates the mean, and the  
 750 red line indicates the median; the kernel bandwidth was 0.05.

751